Journal of Infrared, Millimeter, and Terahertz Waves (2026) 47:25
https://doi.org/10.1007/s10762-026-01147-y

RESEARCH

Enabling High Sensitivity Patch-Antenna-Coupled TeraFETs for the Above 1-THz Frequency Band Using Superstrate Lenses

Jakob Holstein[1] · Dmytro B. But[2,3] · Anastasiya Krysl[1] · Alvydas Lisauskas[1,4,5] · Hartmut G. Roskos[1]

Received: 9 March 2026 / Accepted: 25 May 2026 / Published online: 5 June 2026

Abstract

Antenna-coupled field-effect transistors (TeraFETs) have emerged as a class of room-temperature THz detectors capable of competing with Schottky-barrier diodes in sensitivity and response speed. A key advantage of FET-based detectors is their compatibility with mature semiconductor foundry processes, enabling scalable, high-yield fabrication (e.g., 65-nm Si CMOS). Quasi-optical detectors employing planar, ground-plane-free antennas achieve maximum responsivity under substrate lens illumination. However, resonant patch-antenna-coupled FETs cannot employ this configuration due to the presence of a buried metallic ground plane. In [1], we introduced superstrate-coupling strategies for patch antenna-coupled FET resonant at 580 GHz. Here, we investigate eleven front-side-illuminated, superstrate lens-coupled detectors with resonance frequencies between 0.5 and 2.5 THz. A key result is that the minimum *optical* noise-equivalent power (NEP)—defined relative to the total incident beam power—around the resonance frequencies increases significantly less with frequency than in waveguide-coupled Schottky-barrier diode technology. While the investigated detectors exhibit slightly higher NEP below 1 THz, they outperform commercial Schottky-barrier diodes above 1.5 THz. Compared with TeraFETs employing broadband antennas, patch-coupled FETs provide substantially improved performance at their resonance frequencies. Minimum optical NEP values between 16 $\mathrm{pW}/\sqrt{\mathrm{Hz}}$ at 0.52 THz and 43 $\mathrm{pW}/\sqrt{\mathrm{Hz}}$ at 2.45 THz were achieved and confirmed by broadband thermal radiation measurements. The results are further compared with substrate-lens-coupled detectors employing log-spiral and other broadband antennas reported in the literature.

Keywords 65-nm CMOS · Field-effect transistor · Radiation · THz detection · Superstrate lens · Passive sensing

Extended author information available on the last page of the article

1 Introduction

Over the past decade, antenna-coupled field-effect transistors (TeraFETs) have been extensively studied as fast, sensitive power detectors [2–5] and coherent mixers [6–8] for diverse applications. Their detection mechanism—based on plasma-wave-assisted resistive mixing [9] with additional contributions from the photothermoelectric effect [10]—enables implementation in various material systems, including Si CMOS [11, 12], AlGaAs/GaAs [13, 14], AlGaN/GaN [15, 16], graphene [10, 17, 18], and even carbon nanotubes [19]. Antennæ, for TeraFETs, are selected based on application requirements and are broadly categorized as broadband (e.g., log-spiral or bow-tie antennas) [15, 20] or narrowband (e.g., biquad, patch, or slot-dipole antennas) [4, 11, 21]. Patch antennæ, in particular, are comparatively compact, requiring a relatively small area, which favors the realization of high pixel densities in array configurations for both power [22–26] and heterodyne detection schemes [27]. At the frequencies considered here, their three-dimensional geometry (resulting from the combination of the metallic patch with a buried ground-plane [9, 28]) lends itself for implementation in the back-end of standard foundry-based Si CMOS process technology. Patch antennæ feature narrow spectral widths (full width at half maximum (FWHM): 8% to 10% of their resonance frequency ν_{res}) in the investigated frequency range. They exhibit a high impedance at ν_{res}, which is primarily determined by the length of the patch L_p.

Recent advancements have expanded the applicability of TeraFETs to domains such as scanning near-field optical microscopy (s-SNOM) [29], 250-GHz communication systems [30], multi-spectral imaging [31, 32], high-resolution gas-phase spectroscopy [33, 34], passive (thermal) detection and imaging [35], and the detection of ultrashort laser pulses [36–38]. Of particular interest is the detection of multi-THz radiation from quantum cascade lasers (QCLs). In the 2–5-THz band, TeraFETs have been deployed as QCL power monitors [28] and as detectors of QCL radiation used for static gas spectroscopy [26, 33, 34] as well as for real-time investigation of dynamic gas-phase phenomena [34, 39].

Despite their advantages, single patch-antenna-coupled TeraFETs face limitations, such as small effective antenna areas and buried ground-planes, the latter precluding substrate-side illumination. For TeraFETs with patch antennæ at 500 GHz, these challenges have been addressed through superstrate lens techniques [1], achieving a state-of-the-art optical NEP of 16 pW/Hz$^{0.5}$ at 528 GHz—surpassing the NEP of broadband quasi-optical detectors. Leveraging the large frequency coverage and high spectral resolution of a continuous-wave (*cw*) photomixer-based spectroscopy system, we present a systematic study of superstrate-lens coupling for ten patch-antenna-coupled TeraFETs, with resonance frequencies spanning 0.5–2.45 THz, measuring the optical NEP spectra of the detectors. In addition, we determine their NEP values via measurements of thermal radiation from a heated membrane-type emitter following the approaches of [35, 40].

2 Detector Design, Fabrication, and Packaging

2.1 Design and Fabrication

The TeraFETs characterized in this study were fabricated using a commercial 65-nm Si CMOS process (Taiwan Semiconductor Manufacturing Company, TSMC). Detector designs were developed in the Cadence Virtuoso environment, while the three-dimensional patch antenna structures were simulated using CST Microwave Studio. System-level electrical characteristics, including transistor–antenna interactions, were modeled and optimized for minimum NEP using Keysight Advanced Design System 2022 (ADS). A detailed description of the applied simulation methodology, together with a comparison between simulated and experimental results for patch-antenna-coupled TeraFETs, is provided in [9]. Note that the chip design and the ensuing resonance frequencies presented here differ from those of [1].[1]

The implemented die (thickness, 270 μm) integrated ten patch-antenna-coupled TeraFETs, shown at the top of Fig. 1 (labeled A1–A10), with patch lengths ranging from 20 to 138 μm, corresponding to resonance frequencies of 0.52–2.45 THz. Because the patch antenna is embedded in metal layer M10, the separation between the ground plane (M2) and the patch is $h = 8.4\,\mu\text{m}$. A cross-sectional view of the implemented antennas in the same 65-nm process is provided in [9] (Fig. 1b). The channel length of the transistor's gate was uniformly 60 nm, while the channel widths vary between 200 nm and 1 μm for optimal impedance matching. Patch geometries and transistor parameters are summarized in Table 1. The detector labeled B5 at the top of Fig. 1 is part of a chip fabricated for the studies of [1].

2.2 Device Packaging Including Attachment of Substrate Lens

The chip with the TeraFETs was mounted on a printed circuit board (PCB) and wire-bonded, connecting the detectors' source, drain, and gate contacts to external SMA connectors. With regard to the attachment of the superstrate lens, we combined the approach of type *B* and type *C* in [1]. The fragile bonding wires were embedded in a thermally curable epoxy (EPO-TEK 353ND) for mechanical protection [1]—keeping the thickness of the epoxy bumps below 250 μm. The antenna of the TeraFETs was left uncovered. On these, a thin paraffin layer (approximately 100 μm thick, $\epsilon_R \approx 2.3$) was applied by drop casting [41], into which a 150-μm-thick stripe of highly resistive Si (undoped, $\rho > 10\,\text{k}\Omega\,\text{cm}, n = 3.41$) was softly pressed during the cooling period. The silicon slab—after application of a small amount of silicone grease (KORASILON, middle viscosity)–served then as the basis for the mounting of a hyper-hemispherical

[1] The die shown in [1] represents an earlier chip generation fabricated in the same TSMC 65-nm process. The designs differ primarily in the implemented patch geometries, resulting in different resonance frequencies and spectral characteristics. In addition, the antenna implementations in the previous fabrication run included supplementary passive patches in lower metal layers to satisfy the 65-nm process metal-density requirements. These structures introduced undesired spectral features and were therefore omitted in the present generation.

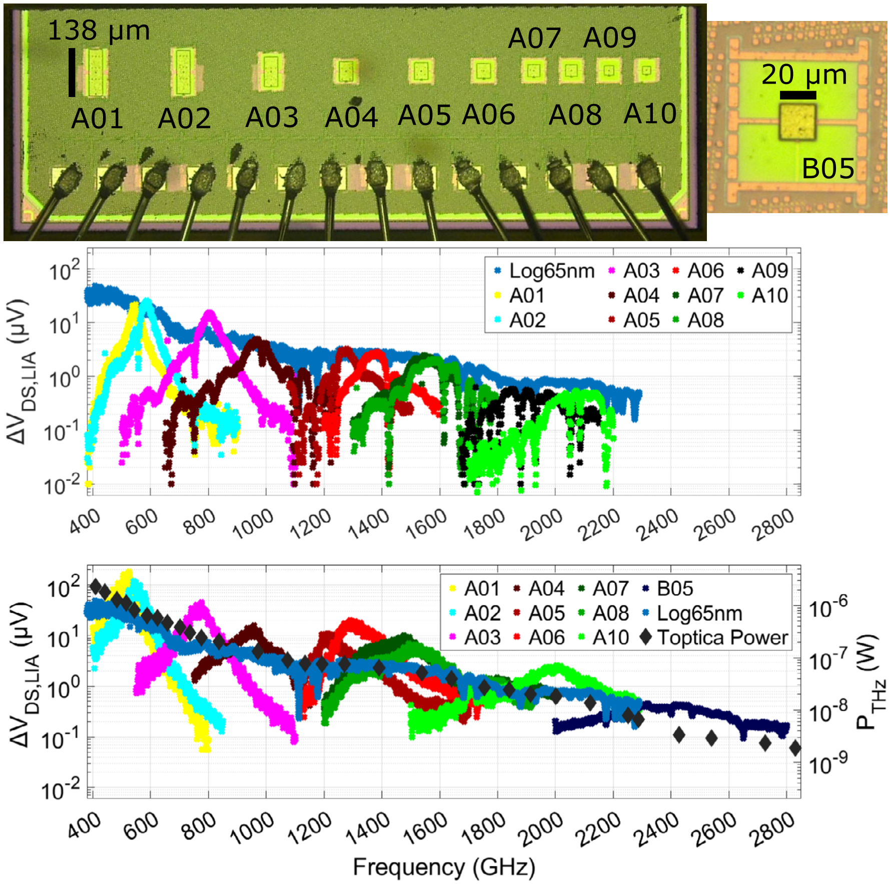

Fig. 1 *Top, left side:* Detector chip featuring ten patch-antenna-coupled TeraFETs labeled A01 to A10. The lengths of the patch antennæ range from 23.5 to 138 µm corresponding to resonance frequencies of 0.54 to 2.1 THz (without a superstrate lens). Additional parameters are listed in Table 1. The bonding pads and the 25-μm-thick Al bonding wires are visible at the bottom of the chip. The overall chip dimensions are $2\times1\,\text{mm}^2$. *Top, right side:* Separate patch-antenna-coupled TeraFET B05 from a chip fabricated for [1]. Patch length, 20 μm; resonance frequency, 2.45 THz (with Si-lens). *Center:* Unprocessed spectral response data acquired for all ten detectors **without** a Si superstrate lens. Data obtained using a photomixer emitter; the detectors were placed at the focus of a 2-inch off-axis paraboloidal mirror. No purging with dry N_2 was applied for the suppression of absorption by water vapor in the air. *Bottom:* Unprocessed spectral response data of the detectors equipped **with** a Si superstrate lens, measured under a dry N_2 atmosphere. The measured terahertz rectified drain–source voltage, $V_{\mathrm{DS,LIA}}$, corresponds to the signal directly recorded by the lock-in amplifier. The decrease in $V_{\mathrm{DS,LIA}}$ at higher frequencies is primarily attributed to the pronounced roll-off in the available output power of the employed photomixer emitter (see Appendix Fig. S2 for the applied procedure used to determine the available $P_{\mathrm{THz}}(\nu)$). The corresponding voltage responsivities are shown in Fig. 3. For reference, the available emitter power is indicated by the black diamonds in the bottom panel (right y-axis). The dark-blue line represents the spectral response of a TeraFET with a log-spiral antenna, also fabricated in the same 65-nm foundry technology and equipped with a Si substrate lens

Si-lens (diameter, $2r = 4$ mm; height, $h = 2.2$ mm) to the respective detector. The height of the silicon slab was chosen to approach the condition

$$t = \frac{n+1}{n} \cdot r \tag{1}$$

of an aplanatic hyper-hemispherical lens (coma-free planar phase front in the antenna plane) [42]. Here, t is the distance from the apex of the lens to the focal point.

A schematic of the finished device is displayed in the inset of the left panel of Fig. 2. Detectors A1 to A10 were integrated and tested within the same die (see Fig. 1). The described mechanical system enabled characterization of all ten detectors integrated on the die in separate measurement runs by positioning the respective detector under test at the focal point of the lens using a precision X–Y translation stage (Thorlabs ST1XY-D). For the characterization of an individual detector, the antenna position was adjusted, while the lens position remained fixed, to maximize the THz response within the focal region of the optical system shown in Fig. 2; the remaining detectors were disabled.

3 Experimental Techniques

3.1 DC Current–Voltage Characterization

To characterize the transistors' current–voltage (IV) behavior, we applied a source-drain bias of $V_{DS} = \pm 10$ mV and measured the source-drain current as a function of gate-source voltage ($V_{GS} = 0V to 1V$). From these IV measurements, we derived the drain-source resistance, $R_{DS}(V_{GS})$, for each detector using a two-channel source-measure unit (SMU; Keysight 2902B). $R_{DS}(V_{GS})$ was later employed for the determination of the optical NEP [15] under unbiased source-drain conditions ($V_{DS} =$

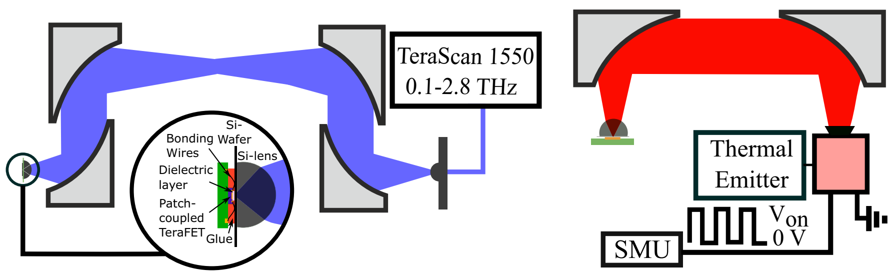

Fig. 2 Schematic views of the two experimental setups for the determination of the TeraFETs' responsivity. *Left panel:* Setup for measurements with tunable narrowband THz radiation using an optoelectronic radiation source. The beam (shown in blue, propagation from right to left) is guided to the TeraFET with the help of four OAP mirrors (with an intermediate focus, which can be employed for spectroscopic purposes). To minimize THz absorption by air humidity, the beam path is purged with dry nitrogen gas. Inset: Cross-sectional schematic view of the TeraFET with a superstrate lens. *Right panel:* Setup for measurements with thermal radiation emitted by a periodically biased heat source. The beam path (shown in red, beam propagation from right to left) was purged by dry nitrogen gas during the measurements

0 V), because the noise spectral density V_N is then dominated by Johnson-Nyquist thermal noise according to [43]

$$V_N(V_{GS}) = \sqrt{4k_B T\, R_{DS}(V_{GS})}, \tag{2}$$

with $k_B = 1.38 \times 10^{-23}$ J K^{-1} being Boltzmann's constant and $T = 293$ K the detector temperature (all experiments were performed at room temperature).

3.2 Experimental Setup and Methods for the Determination of the NEP with Tunable Narrow-Band Radiation

For the measurement of the THz responsivity, we employed two different radiation sources: narrow-band radiation from a cw photomixer and broadband radiation from a thermal emitter. For the measurements with the former, we modified a *cw*-THz spectroscopy system (Toptica TeraScan 1550) by replacing its detector with the TeraFETs (left panel of Fig. 2). The spectroscopy system is based on three 1550-nm DFB lasers covering slightly different spectral emission bands. Any two can be combined for difference-frequency generation in an InGaAs photomixer to cover the target frequency range from 60 to 2850 GHz (low range, 60 to 1200 GHz; middle range, 1030 to 2290 GHz; and high range, 1600 to 2850 GHz) [44]. The bias voltage of the photomixer was electronically modulated with a square-wave signal at $f_{mod} = 7629$ Hz for lock-in detection. The emitted radiation was guided through an optical system consisting of four off-axis paraboloidal (OAP) mirrors, which allow for transmission spectroscopy of materials (see [1] for a measurement on α-lactose powder). The last OAP mirror's reflected focal length (RFL) was chosen to be 2 inches,[2] which is fairly small and was selected to have a small area of the focal spot for a good beam overlap with the patch antenna of the TeraFET even without a superstrate lens. Care was taken to align the TeraFET detector's dipole axis with the linearly polarized radiation. The THz beam path was fully enclosed in a housing to enable efficient purging with dry nitrogen gas during the measurements, thus avoiding absorption of the radiation by water vapor in the air. The detector was operated at zero source-drain bias. The rectified voltage was fed into a lock-in amplifier (LIA, model: AMETEK DSP 7629) with f_{mod} as reference frequency. Based on the LIA output signal V_{DS}, we calculated the detector's frequency-dependent optical voltage responsivity $\mathcal{R}_V(V_{GS}, \nu) = V_{DS}^{p}(V_{GS}, \nu)/P_{THz}(\nu)$. Here, $V_{DS}^{p}(V_{GS}, \nu)$ is the peak signal (i.e., amplitude) of the modulated rectified voltage, and $P_{THz}(\nu)$ the full power (not modulated at f_{mod}) of the radiation impinging onto the detector. For perfect square-wave modulation with 50% duty cycle, the relationship of $V_{DS}^{p}(V_{GS}, \nu)$ to $V_{DS}(V_{GS}, \nu)$, the root-mean-square (RMS) voltage provided by the LIA, is $V_{DS}^{p}(V_{GS}, \nu) = \alpha_{LIA} \cdot V_{DS}(V_{GS}, \nu)$, with $\alpha_{LIA} = \pi/\sqrt{2} \approx 2.2$ [45]. However, when inspected with an oscilloscope, the modulation of the TeraScan's THz wave was found to deviate from the ideal square wave, and a value of $\alpha_{LIA,Toptica} \approx 3$ was derived for the recorded waveform [46]. With this value, we calculated the detector's

[2] OAP mirror's RFL from emitter to detector: OAP1 4-inch, OAP2 6-inch, OAP3 6-inch, and OAP4 2-inch. Diameter 2-inch for each mirror.

optical voltage responsivity, which refers to the full available power within the focal plane with the expression

$$\mathcal{R}_{\mathrm{V,opt}}(V_{\mathrm{GS}}, \nu) = \frac{\alpha_{\mathrm{LIA,Toptica}} \cdot V_{\mathrm{DS}}}{P_{\mathrm{THz}}(\nu)} \,. \tag{3}$$

The frequency-dependent emitted power $P_{\mathrm{THz}}(\nu)$ was measured at the detector position with a calibrated pyroelectric detector (THz 10 HS, SLT Sensor- und Lasertechnik GmbH) and a Golay cell. Their sensitivity limits only allowed to cover the frequency range from 60 to 730 GHz because of the strong frequency roll-off of the emitted power (dropping to approx. 200 nW at 800 GHz). We extrapolated the power towards higher frequencies based on the signal-to-noise ratio (SNR) measured with the system's commercial broadband InGaAs photomixer (see Supplementary Material and [47]). The output power $P_{\mathrm{THz}}(\nu)$ derived in this way is displayed from 400 GHz up to 2.85 THz in the bottom panel of Fig. 1 (white dotted line). We note that care has to be taken when the photomixer's emitted power is determined with broadband detectors such as pyroelectric and Golay-cell-based thermal power meters, and TeraFETs with broadband antenna covering frequencies below 250 GHz. It is known that side-modes of the diode lasers produce spurious photomixing signals at other frequencies than the difference frequency of the main modes [48, 49]. This appears to be dominated by self-mixing in the photomixer device (main line of each laser mixing with its own side-bands) [48, 49]. In case of the TeraScan system, the spurious frequency components are mainly located below 250 GHz and affect mostly measurements at high THz frequency where the power of the radiation is weak [48]. We expect that our extrapolation of the power beyond 730 GHz is not significantly affected by these spurious signals because of the high-pass frequency filtering inherent to the coherent generation and detection of THz radiation with photomixers. Equally, we are confident about the validity of the responsivity measurements because of the resonant (narrow-band) character of the response of the patch antenna.

Having determined the optical voltage responsivity $\mathcal{R}_{\mathrm{V,opt}}(V_{\mathrm{GS}}, \nu)$ as defined in Eq. 3 and the noise spectral density $V_{\mathrm{N}}(V_{\mathrm{GS}})$ (Eq. 2), one calculates the optical $\mathrm{NEP}_{\mathrm{opt}}(V_{\mathrm{GS}}, \nu)$ with the expression

$$\mathrm{NEP}_{\mathrm{opt}}(V_{\mathrm{GS}}, \nu) = \frac{V_{\mathrm{N}}(V_{\mathrm{GS}})}{\mathcal{R}_{\mathrm{V,opt}}(V_{\mathrm{GS}}, \nu)} \,, \tag{4}$$

where the gate bias voltage V_{GS} is chosen for the best sensitivity of the detector (lowest NEP, highest SNR) at its resonance frequency, and not for the highest voltage responsivity $\mathcal{R}_{\mathrm{V,opt}}(V_{\mathrm{GS}}, \nu)$, which would be found at a lower bias voltage (and would be twice higher) but where the noise level is significantly increased [11, 22]. The integration time was chosen with 100 ms in case of the cw-characterizations.

3.3 Experimental Setup and Methods for the Determination of the NEP with Thermal Radiation

In a second series of measurements, we followed an independent way to determine the optical NEP of the detectors from the measured SNR [40], using the thermal radiation from the membrane-type ceramic radiator of [35] (INTX17-0900 [50], active area: 1.7×1.7 mm^2, fitted with a paraboloidal reflector). The active area of the device was periodically heated by an 11-Hz square-wave electrical current to 600 °C using a Tektronix AFG3000 function generator and a Keysight B2902B SMU in pulse mode. The thermal time constant of the device is specified to be 11.4 ms, and the emission spectrum closely follows Planck's law [50].

The thermal radiation was guided from emitter to detector via two OAP mirrors (2-inch diameter and 2-inch focal length) (see right panel of Fig. 2). The rectified signal from the TeraFET (no source-drain bias applied) was fed into a LIA (AMETEK DSP 7265), locked to the 11-Hz square-wave reference, and set to a 1-s integration time T_C and a 6-dB/octave filter slope, resulting in an equivalent noise bandwidth (ENBW) of $\Delta f = 0.25$ Hz [51]).

From the LIA output signals S_k, we determined the SNR of the signals as the ratio $\mathrm{SNR} = \frac{\mu_\mathrm{S}}{\sigma_\mathrm{S}}$ of the mean signal amplitude $\mu_\mathrm{S} = \sum_{k=1}^{\mathrm{N}} S_\mathrm{k}$ and the signal's standard deviation $\sigma_\mathrm{S} = \sqrt{(\sum_{\mathrm{k=1}}^{\mathrm{N}}(S_\mathrm{K} - \mu_\mathrm{S})^2)/N}$, sampled over $k = 1, ..., N$ data points, with $N = 300$ [52]. To obtain N statistically independent samples, a waiting time between the recording of two data points of $4T_C$ was chosen.

From the SNR, the optical NEP of the detectors was obtained in the following way. The SNR is defined by

$$\mathrm{SNR}(V_\mathrm{GS}, \nu) = \frac{V_\mathrm{DS}(V_\mathrm{GS}, \nu)}{V_\mathrm{N}(V_\mathrm{GS}) \cdot \sqrt{\Delta f}}\,. \tag{5}$$

Δf represents the detection bandwidth of the measuring device (here, LIA, with Δf depending on the chosen integration time constant T_C and filter slope; for the DSP7265 model, see [51]). With Eq. 3, one replaces V_DS in Eq. 5 (replacing $\alpha_\mathrm{LIA,Toptica}$ by $\alpha_\mathrm{LIA,thermal}$ taking account of the type of modulation in the experiments with thermal radiation) and obtains with Eq. 4 the relationship

$$\mathrm{NEP}_\mathrm{opt}(V_\mathrm{GS}, \nu) = \frac{P_\mathrm{THz}(\nu)}{\alpha_\mathrm{LIA,thermal} \cdot \mathrm{SNR}(V_\mathrm{GS}, \nu) \cdot \sqrt{\Delta f}}\,, \tag{6}$$

Here, $P_\mathrm{THz}(\nu) = P_\mathrm{bb}(\nu, \Delta\nu, T_\mathrm{max}) - P_\mathrm{bb}(\nu, \Delta\nu, T_\mathrm{min})$ is the modulated part of the power of the black-body radiation, impinging onto the detector within its acceptance cone and integrated over the detector's bandwidth $\Delta\nu$.

In [35], based on [13, 53], it was shown that the power spectral density received by an ideal antenna with an optimally filled beam acceptance cone is a constant, which only depends on the temperature T of the radiator and its emissivity $\epsilon(\nu)$ (which is assumed to be unity in the following). It does not depend on the center frequency ν of the antenna. This surprisingly simple result was obtained from Planck's law of the spectral radiance in the limit of the Rayleigh-Jeans law, which holds for $h\nu \ll k_\mathrm{B}T$, valid for the temperatures and frequencies of this study. The power arriving from the radiator at T is hence given by

$$P_\mathrm{bb}(\Delta\nu, T) = k_\mathrm{B} \cdot T \cdot \Delta\nu \,, \tag{7}$$

with

$$\Delta\nu = \int_{-\infty}^{\infty} \widehat{\mathcal{R}_\mathrm{V}}(\nu)\,\mathrm{d}\nu \,. \tag{8}$$

$\widehat{\mathcal{R}_\mathrm{V}}(\nu)$ refers to the normalized frequency-dependent voltage responsivity, which was determined using the optoelectronic narrow-band measurement system. The modulated power, to be entered into Eq. 4, is then

$$P_\mathrm{THz} = P_\mathrm{bb}(\Delta\nu, T_\mathrm{max}) - P_\mathrm{bb}(\Delta\nu, T_\mathrm{min}) = k_\mathrm{B} \cdot \Delta T(f_\mathrm{mod}) \cdot \Delta\nu \,, \tag{9}$$

where $\Delta T(f_\mathrm{mod}) = \Delta T \cdot D(f_\mathrm{mod})$ describes the effective temperature difference of the periodically heated thermal radiator. ΔT is the nominal temperature difference of 580 K (600 °C minus 20 °C) at the modulation frequency f_mod of 11 Hz. The modulation depth $D(f_\mathrm{mod})$ was experimentally determined to be 0.9 (see Supplementary Material).

Inserting Eqs. 8 and 9 into 6 yields for the optical $\mathrm{NEP}_\mathrm{opt,min}$ at the optimal gate bias voltage V_GS the expression

$$\mathrm{NEP}_\mathrm{opt,min}(\nu) = \frac{k_\mathrm{B} \cdot \Delta T(f_\mathrm{mod})}{\alpha_\mathrm{LIA,thermal} \cdot \mathrm{SNR}(\nu) \cdot \sqrt{\Delta f}} \cdot \int_{-\infty}^{\infty} \widehat{\mathcal{R}_\mathrm{V}}(\nu)\mathrm{d}\nu \,. \tag{10}$$

For $\alpha_\mathrm{LIA,thermal}$, we employed the value $\alpha_\mathrm{LIA,thermal} = \pi/\sqrt{2}$ for square-wave modulation to transform the RMS signals of the LIA to peak-to-peak signals.

4 Experimental Results

4.1 Measurements with Tunable Narrow-Band Radiation

Figure 1 presents results of response measurements with the optoelectronic narrow-band radiation source, depicting as-recorded LIA output voltages for the ten TeraFETs without and with superstrate lenses (upper and bottom panels, respectively, the latter also shows results for device B5). For comparison, measurement data of a TeraFET with a broadband operable log-spiral antenna,[3] fabricated with the same 65-nm foundry technology as the other TeraFET detectors and carrying a substrate lens, are depicted as well.

[3] FET-parameters: W_ch = 0.7 µm, L_g = 60 nm, L_ug = 55 nm. Antenna parameters: Inner Radius: 10 µm/15 µm, outer radius 412 µm. Windings: 1.5. Antenna is implemented in AP-layer(M10). Resulting length of the vias is 8.4 µm (compare cross-sectional view in [9]). Impedance simulations of the antenna can be found in [54].

By direct comparison of the data in the two panels, one finds that the application of a superstrate lens led to an increase in the rectified signal of approx. $8 - 10$ dB across all detectors. Note that the tighter focusing of the THz radiation by the lens also introduced more pronounced standing waves on the rectified signal (from waves being reflected off the ground plane of the antenna back towards the radiation source). Their modulation frequency is too high to be visible in the main panel, where the data curves simply appear thicker for the devices with a superstrate lens, but the modulation is spectrally resolved in the magnified view on the A03 curve shown in the inset in the bottom panel of Fig. 5 in the Supplementary material.

A comparison of the response data of the patch-antenna-equipped devices with those of the detector with log-spiral antenna (bottom panel of Fig. 1) shows that the narrow-band detectors exhibit the expected superior performance at their resonance frequencies.

With the frequency dependence of the radiation power as shown by the white dotted line in the bottom panel of Fig. 1, we corrected the response curves of the devices for the spectral characteristics of the radiation and determined the spectra of the responsivity and of the optical NEP. Figure 3 presents the frequency-dependent voltage responsivity $\mathcal{R}_V(\nu)$ (upper panel) and of the optical NEP (lower panel) of ten patch-TeraFETs with superstrate lenses and of the log-spiral antenna-coupled TeraFET with substrate Si-lens.[4]

A remarkable and central result is the lack of a significant frequency dependence of the peak values of $\mathcal{R}_V(\nu)$ of the ten detectors over the entire frequency range. Only above 1.5 THz, one can speculate about slightly decreased peak $\mathcal{R}_V(\nu)$ values, which may result from a somewhat less efficient coupling of the signal to the transistor channel. Compared with the detector with a log-spiral antenna, which exhibits a gradual rise in responsivity with frequency, all patch-TeraFETs except B05 significantly exceed its $\mathcal{R}_V(\nu)$ values at their respective resonances. Note that—at 2.5 THz—B05 and the TeraFET with log-spiral antenna also show a higher responsivity than the GaAs Schottky detectors described in [55–57] (the sensitivity of the diodes is commonly expressed in the literature in terms of *video responsivity*, which is directly comparable to $\mathcal{R}_V(\nu)$ of this work). For comparison, the B05 detector (without a lens) was characterized in the focal plane of a 2.5 THz QCL delivering 2 mW of available terahertz power. The corresponding cross-sectional NEP, determined from a scan across the QCL focal plane as described in [30], is presented in the bottom panel of Fig. 3. The optical NEP spectra, shown in the lower panel of Fig. 3, exhibit a correspondingly stable behavior of the minimum NEP values at the respective resonance frequencies. These minimum NEP values are also summarized in Table 1, distinguishing between $\mathrm{NEP}_{\mathrm{opt,min,a}}$, the standing-wave–averaged values (white lines in Fig. 3), and $\mathrm{NEP}_{\mathrm{opt,min,b}}$, the peak values of the raw data (where one takes advantage of the increased dynamic range resulting from the standing waves).[5] Over the entire frequency range, the $\mathrm{NEP}_{\mathrm{opt,min,a}}$ values only vary between 22 $\mathrm{pW}/\sqrt{\mathrm{Hz}}$ (A03, 775 GHz) and 52 $\mathrm{pW}/\sqrt{\mathrm{Hz}}$ (A08, 1.53 THz). The respec-

[4] Detector A09 could not be characterized while being coupled to a superstrate lens as the A09's FET-element broke during the experimental phase.

[5] This effect has been used in spectroscopy applications to resolve a particular spectroscopic feature (compare [59]).

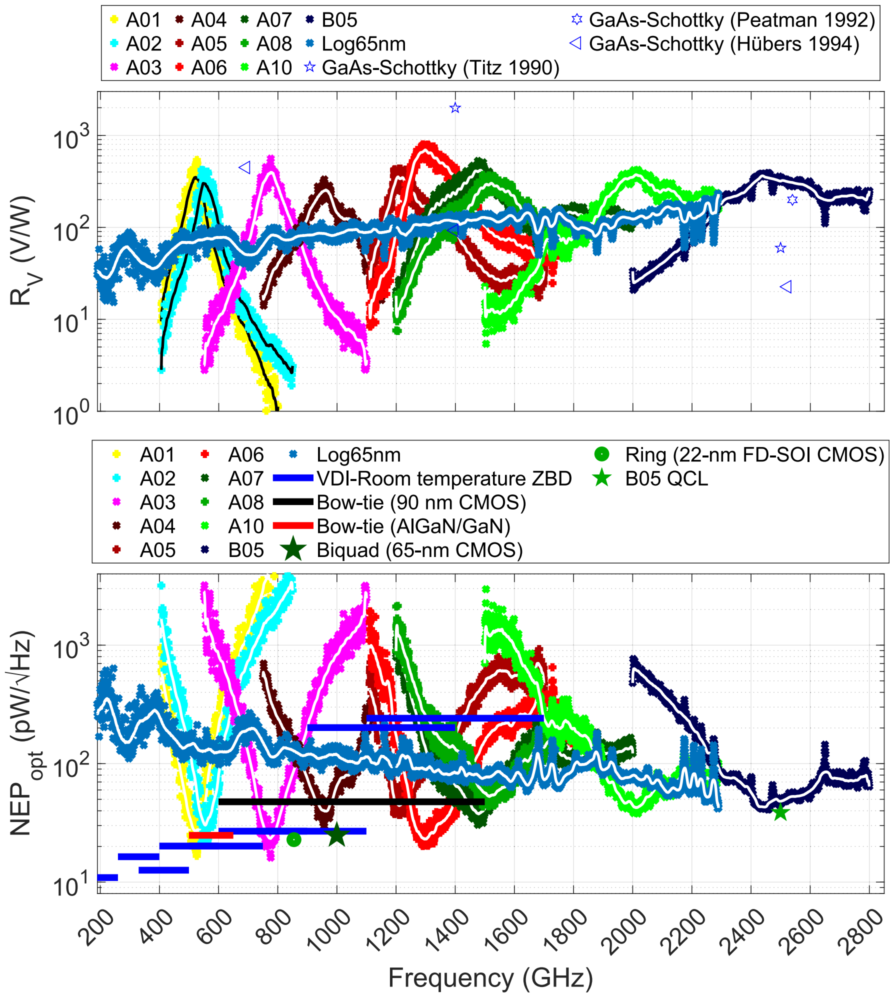

Fig. 3 Frequency-dependent optical voltage responsivity (upper panel) and optical NEP (bottom panel) of ten patch-TeraFETs with superstrate lenses. The white lines are the sliding frequency averages over the standing-wave modulations in the curves. Performance parameters of the TeraFETs in this graph are summarized in Table 1. The top and bottom panels also show data for other types of power detectors from the following references: [55–57] in the top panel, [15, 20, 21, 58] in the bottom panel. For further details, see the main text. In addition, experimental cross-sectional NEP results for B05-detector in the focal plane of a 2.5 THz QCL are indicated

tive $\mathrm{NEP}_{\mathrm{opt,min,b}}$ values vary between 16 pW/$\sqrt{\mathrm{Hz}}$ (A01, 525 GHz) and 44 pW/$\sqrt{\mathrm{Hz}}$ (A08, 1.53 THz). Even the values for the patch-TeraFET with the highest resonance frequency of 2.45 THz remain within these boundaries: $\mathrm{NEP}_{\mathrm{opt,min,a}} = 45$ pW/$\sqrt{\mathrm{Hz}}$, respectively $\mathrm{NEP}_{\mathrm{opt,min,b}} = 43$ pW/$\sqrt{\mathrm{Hz}}$.

The lower panel of Fig. 3 also provides comparative literature data of the optical NEP of other power detectors. Among these are four substrate-lens-equipped TeraFETs and a series of zero-bias Schottky diodes (ZBDs).

Of the TeraFETs, one is a GaN/AlGaN TeraFET with bow-tie antenna [15] (symbol, red bar; optical NEP, $25-31$ pW/$\sqrt{\text{Hz}}$ in 0.49–0.65 THz). The other three are Si CMOS TeraFETs with (i) a narrow-band ring antenna [58] (symbol, green dot; optical NEP, 22.7 pW/$\sqrt{\text{Hz}}$ at 0.855 THz, voltage-mode readout), (ii) a semi-broadband biquad antenna [21] (symbol, green star; optical NEP, 25 pW/$\sqrt{\text{Hz}}$ at 1.0 THz), and (iii) an ultra-broadband bow-tie antenna [20] (symbol, black horizontal bar; optical NEP, $48-70$ pW/$\sqrt{\text{Hz}}$ at $0.6-1.5$ THz (full operation range, 0.4−2.2 THz)). The patch-TeraFETs with superstrate lenses considered in this work compare well with these devices, which are considered the best-performing TeraFETs. For the comparison with Schottky-diode-based power detectors, we considered ZBD detectors from Virginia Diodes Inc. (VDI), taking performance data from [60] for devices embedded in various types of waveguides. The data are plotted in Fig. 3 as blue horizontal bars. Below 0.6 THz, the ZBD detectors demonstrate a slightly better optical NEP than our devices at their resonance peaks, but with values >10 pW/$\sqrt{\text{Hz}}$, their advantage is not significant as it is with regard to TeraFETs with broadband antennas. However, at about 1 THz, a crossover occurs, where the NEP performance of our TeraFETs becomes superior and the ZBD detectors fall behind even in comparison with the broadband TeraFET of Fig. 3. While the TeraFET devices exhibit a sensitivity decrease of approximately a factor of two between 1 and 2.5 THz, the loss in performance is significantly more pronounced for the Schottky-based detectors.

In the frequency range above 1.6 THz, literature on Schottky-based power detectors is extremely limited, as these devices are predominantly employed as heterodyne mixers in combination with powerful local oscillators. While occasionally the optical responsivity is reported [55–57, 61], more commonly the sensitivity of a detector is characterized by the noise temperature, which strongly depends on the local oscillator power and the overall system's noise performance. An exception is the Schottky power detectors reported in [62, 63]. They are both operated in quasi-optical mode. The former reference reports about a GaAs ZBD detector of ACST GmbH with optical NEP values of 10 pW/$\sqrt{\text{Hz}}$ at $0.2-0.6$ THz, 17 pW/$\sqrt{\text{Hz}}$ at 1.2 THz, and 900 nW/$\sqrt{\text{Hz}}$ at 5.56 THz. The latter describes an antenna-coupled CMOS Schottky diode, which achieved an optical NEP of 430 pW/$\sqrt{\text{Hz}}$ at 4.92 THz and 1.1 nW/$\sqrt{\text{Hz}}$ at 9.74 THz.

4.2 Measurements with Thermal Radiation

Thermal radiation emitted by the ceramic membrane-type black-body emitter, periodically heated at a repetition rate of 11 Hz, could be sensed with sufficient SNR, despite the narrow spectral width $\Delta\nu_{\text{res}}^{\text{FWHM}}$ of the respective patch-antenna's resonance. The respective detector's $\Delta\nu_{\text{res}}^{\text{FWHM}}$ are listed in Table 1 (as $\Delta\nu_{\text{res}}^{\text{FWHM}}$). Here, full width at half maximum (FWHM) was determined from the voltage responsivity curves shown in Fig. 3. Results of the measurements and data processing following Sect. 3.3 are displayed in Fig. 4. In the left panel, the experimentally determined SNR is displayed for detectors A01 to A08 and A10.[6] The data were recorded with a LIA integration time of 1 s. Also, the effective linewidth $\Delta\nu_{\text{Eq.8}}$ of the detectors, calculated with Eq. 8, is displayed. The values are also listed in Table 1. The values are in a reasonable

[6] For detectors A09 and B05, no thermal experiments were performed.

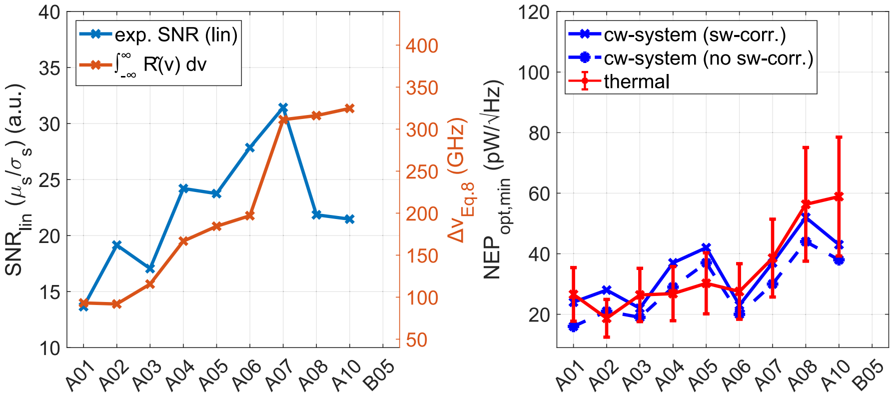

Fig. 4 *Left panel:* Experimentally determined SNR for the patch-antenna-coupled TeraFETs A01-A08 and A10, all with superstrate lens (blue data points). The measurements were performed with the beam path purged with dry N_2 gas. Spectral width $\Delta\nu_{res}^{FWHM}$ represents the antenna's FWHM (red data points). The spectral bandwidth calculated via Eq. 8 is shown in Table 1. *Right panel:* Comparison of the minimum optical NEP values determined with tunable narrow-band radiation (blue data points, with and without averaging over the standing-wave modulations) and with thermal radiation (red data points with error bars)

relationship to each other which supports the validity of the analytical approach of Sect. 3.3. The main result of the thermal measurements is displayed on the right side of Fig. 4. The red symbols show the values of the minimum optical NEP as determined with Eq. 10. They are compared with the corresponding values extracted from Fig. 3 (with and without averaging over the standing-wave modulations). There is a good agreement between the two datasets. Both show the weak spectral dependence of the minimum NEP with the slight increase above 1.5 THz (A07 onwards). The comparison also leads to the conclusion that measurements with thermal radiation can provide a reliable way for the determination of $NEP_{opt,min}$ of a detector, provided the detector's effective absorption bandwidth is known. Finally, we present in Table 1 the values of the corresponding noise-equivalent temperature difference (NETD) calculated by the expression $NETD = NEP \cdot \sqrt{\Delta f}/(\langle\epsilon\rangle k_B \Delta\nu)$ [35] for detectors A01–A08 and A10. Values are given for both the equivalent noise bandwidth (ENBW) of $\Delta f = 0.25$ Hz of our experiments (listed as "NETD (exp)") and for a hypothetical bandwidth of 1 Hz. The latter values vary between 15 and 34.2 K. These are to be compared with the 5.1 K obtained in [35] with a broadband TeraFET detector (log-spiral antenna) from [20]. The patch-TeraFETs are clearly inferior to the broadband device of [35], and their superior responsivity at the resonance peaks cannot compensate for the limited detection bandwidth. Despite uncertainties, such as exact knowledge of the emitter's frequency-dependent emissivity, a relatively good comparability between the detector's NEP being calculated from two different measurements can be reported. The presented comparison can be useful for metrology techniques to verify experimental optical NEP obtained with *cw*-systems in combination with a well-known black-body emitter.

Table 1 Summary of TeraFET parameters and their respective spectral response with and without Si-lens (for details, see main text). All transistors were implemented in TSMC's 65-nm technology (1.2VmLowVtMOS)

Det	A01	A02	A03	A04	A05	A6	A07	A08	A09	A10	B05
L_{patch} (μm)	138	130	89	58	50	44	36	34	28	23.5	20
W_{patch} (μm)	40	40	40	40	40	40.5	36	34	28	23.5	20
W_{ch} (nm)	1000	1000	1000	450	200	200	200	200	200	200	200
L_{g} (nm)	60	60	60	60	60	60	60	60	60	60	60
R_{DS} (kΩ)	5	5	5	6	16	16	16	16	16	16	16
V_{GS} (V)	0.55	0.55	0.55	0.60	0.60	0.60	0.60	0.60	0.60	0.60	n.d
no Si-lens											
ν_{res} (THz)	0.54	0.58	0.8	0.98	1.28	1.39	1.54	1.58	1.73	2.08	n.d
$\Delta\nu_{res,abs}^{\mathrm{FWHM}}$ (THz)	0.04	0.05	0.07	0.09	0.07	0.12	0.12	0.12	0.15	0.16	n.d
$\Delta\nu_{\mathrm{res,rel}}^{\mathrm{FWHM}}$	7.3%	7.8%	8.8%	9.2%	5.5%	8.6%	7.5%	7.6%	8.7%	7.7%	n.d
with Si-lens											
ν_{res} (THz)	0.525	0.547	0.775	0.955	1.21	1.295	1.478	1.53	n.d	2.0	2.45
$\Delta\nu_{\mathrm{res,abs}}^{\mathrm{FWHM}}$ (THz)	0.059	0.052	0.082	0.11	0.081	0.122	0.13	0.164	n.d	0.21	0.3
$\Delta\nu_{\mathrm{res,rel}}^{\mathrm{FWHM}}$	11.2%	9.5%	10.6%	11.5%	6.7%	9.4%	8.8%	10.7%	n.d	10.5%	12.2%
$\Delta\nu_{\mathrm{Eq.8}}$ (THz)	0.093	0.092	0.115	0.167	0.184	0.197	0.311	0.316	n.d	0.325	n.d
$\mathcal{R}_{\mathrm{V,opt,a}}$ (V/W)	326	300	374	252	372	696	430	307	n.d	375	363
$\mathrm{NEP}_{\mathrm{opt,min,a}}$ (pW/Hz$^{0.5}$)	24	28	22	37	42	23	37	52	n.d	43	45
$\mathcal{R}_{\mathrm{V,opt,b}}$ (V/W)	540	416	515	332	434	788	527	351	n.d	419	385
$\mathrm{NEP}_{\mathrm{opt,min,b}}$ (pW/Hz$^{0.5}$)	16	21	19	29	37	20	30	44	n.d	38	43
NETD (1Hz) (K)	34.3	24.5	27.5	19.4	19.8	16.9	15.0	21.2	n.d	21.9	n.d
NETD (exp.) (K)	17.2	12.3	13.8	9.7	9.9	8.4	7.5	10.8	n.d	10.9	n.d

5 Summary

We have investigated the improvement of the performance of patch-antenna-coupled TeraFET power detectors by the application of silicon superstrate lenses. The resonance peaks of the detectors (with the lenses) span the frequency range from 525 GHz to 2.45 THz. The Si-lens improves the responsivity and the minimum optical noise-equivalent power by 8 to 10 dB by improving the antenna's effective area and coupling efficiency. This study has allowed us to investigate in detail the frequency dependence of the sensitivity of patch-TeraFETs, which were fabricated with the same 65-nm CMOS foundry technology. The design of each detector has been optimized for maximal sensitivity at its respective resonance frequency. It is found that (i) the sensitivity at resonance does not change much from detector to detector. Over the entire frequency range, the performance only decreases by a factor of two, which may be rather a consequence of the lens alignment, which becomes more difficult at higher frequencies, than of intrinsic reasons. It is also found (ii) that the detectors achieve record sensitivity, with the best NEP as low as 16 $\mathrm{pW}/\sqrt{\mathrm{Hz}}$.

The comparison with literature values of power detectors based on Schottky diodes indicates that the latter are superior up to roughly 1.0 THz, but become inferior above. It is interesting to note that the Schottky detectors are waveguide-coupled, which is commonly thought to lead to better performance than quasi-optical operation of detector devices, as in the case of our TeraFETs. This raises the question of whether this benefit only holds for low frequencies (if at all). It would be interesting to perform a comparison of the two types of devices on equal footing regarding power coupling.

Finally, we point out specific application options for the patch-TeraFETs. Due to the narrow spectral width of the patch antenna, they are well suited for multi-spectral sensing techniques as suggested in [32]. Detector A10, for example, with its resonance at 2.0 THz, appears to be well-suited for experiments investigating the 2.06-THz neutral oxygen transition $^3\mathrm{P}_0 \rightarrow {}^3\mathrm{P}_1$ in the atmosphere [64]. Another use case is telecommunication. The detector with the highest resonance frequency at 2.45 THz could be useful for future wireless communication applications currently investigated with quantum cascade lasers operating around 2.4 THz [65]. We conclude with the reminder that the TeraFETs, with their ultra-high speed of response, lend themselves to heterodyne operation and other coherent modes of detection.

Supplementary Information The online version contains supplementary material available at https://doi.org/10.1007/s10762-026-01147-y.

Author Contribution J. H. led the investigation and contributed to the methodology, software development, validation, visualization, data curation, and wrote the original manuscript. D. B. B. contributed to the investigation and validation. A. K. participated in the investigation. A. L. and H. G. R. conceived and designed the study, developed the methodology, acquired funding, and supervised the project. In addition, H. G. R. contributed to the writing of the manuscript. All authors have read and approved the final manuscript.

Funding Open Access funding enabled and organized by Projekt DEAL. The German team acknowledges Deutsche Forschungsgemeinschaft (DFG) for grant RO 770/43-1 of the trilateral Fraunhofer-DFG transfer project program as well as RO 770 49-1, a project of the INTEREST collaborative research program. A.L. thanks the Research Council of Lithuania (LMTLT), project "Centre of Competence for Terahertz and Hybrid Semiconductor Chips". D.B. acknowledges funding by the European Union (ERC "TERAPLASM," project number: 101053716) and the European Regional Development

Fund (the PolFEL project No. KPOD.01.18-IW.03-0019/23). Views and opinions expressed are those of the author(s) only and do not necessarily reflect those of the European Union or the European Research Council. Neither the European Union nor the granting authority can be held responsible for them.

Data Availability Data available at Zenodo repository: DOI: https://doi.org/10.5281/zenodo.18800146.

Materials Availability Not applicable

Code Availability Not applicable

Declarations

This manuscript builds upon preliminary work presented at the IRMMW-THz conference 2024 in Perth, Australia, DOI: https://doi.org/10.1109/irmmw-thz60956.2024.10697756 [47]. For the purpose of open access, the authors have applied a Creative Commons Attribution (CC BY) license to any Author Accepted Manuscript version arising from this submission.

Ethics Approval and Consent to Participate Not applicable

Consent for Publication Applicable

Conflict of Interest The authors declare no competing interests.

References

1. A. Krysl, D. B. But, K. Ikamas, J. Holstein, A. Shevchik-Shekera, H. G. Roskos, and A. Lisauskas. "Si Superstrate Lenses on Patch-Antenna- Coupled TeraFETs: NEP Optimization and Frequency Fine-Tuning". In: *IEEE Sensors Journal* 24.21 (Nov. 2024), pp. 33872–33880. ISSN: 1530-437X, 1558-1748, 2379-9153. https://doi.org/10.1109/JSEN.2024.3445140. URL: https://ieeexplore.ieee.org/document/10666089/ (visited on 11/03/2024).
2. D. B. But, A. V. Chernyadiev, K. Ikamas, C. Kołaciński, A. Krysl, H. G. Roskos, W. Knap, and A. Lisauskas. "Compact terahertz devices based on silicon in CMOS and BiCMOS technologies". pl. In: *Opto-Electronics Review* (Jan. 2024). ISSN: 1896-3757. https://doi.org/10.24425/opelre.2023.144599. URL: https://journals.pan.pl/dlibra/publication/144599/edition/126923/content (visited on 11/12/2024).
3. G. Valušis, A. Lisauskas, H. Yuan, W. Knap, and H. G. Roskos. "Roadmap of Terahertz Imaging 2021". en. In: *Sensors* 21.12 (June 2021), p. 4092. ISSN: 1424-8220. https://doi.org/10.3390/s21124092. URL: https://www.mdpi.com/1424-8220/21/12/4092 (visited on 11/01/2023).
4. M. M. Wiecha, R. Kapoor, A. V. Chernyadiev, K. Ikamas, A. Lisauskas, and H. G. Roskos. "Antenna-coupled field-effect transistors as detectors for terahertz near-field microscopy". en. In: *Nanoscale Advances* 3.6 (2021), pp. 1717–1724. ISSN: 2516-0230. https://doi.org/10.1039/D0NA00928H. URL: http://xlink.rsc.org/?DOI=D0NA00928H (visited on 07/05/2023).
5. P. Hillger, J. Grzyb, R. Jain, and U. Pfeiffer. "Terahertz imaging and sensing applications with silicon-based technologies". In: *IEEE Transactions on Terahertz Science and Technology* 9.1 (Jan. 2019), p. 1. https://doi.org/10.1109/TTHZ.2018.2884852.

6. H. Yuan, D. Voß, A. Lisauskas, D. Mundy, and H. G. Roskos. "3D Fourier imaging based on 2D heterodyne detection at THz frequencies". en. In: *APL Photonics* 4.10 (Oct. 2019), p. 106108. ISSN: 2378-0967. https://doi.org/10.1063/1.5116553. URL: https://pubs.aip.org/app/article/4/10/106108/1065284/3DFourier-imaging-based-on-2D-heterodyne (visited on 01/14/2025).
7. D. Glaab, S. Boppel, A. Lisauskas, U. Pfeiffer, E. Öjefors, and H. G. Roskos. "Terahertz heterodyne detection with silicon field-effect transistors". en. In: *Applied Physics Letters* 96.4 (Jan. 2010), p. 042106. ISSN: 0003-6951, 1077-3118. https://doi.org/10.1063/1.3292016. URL: https://pubs.aip.org/apl/article/96/4/042106/131998/Terahertz-heterodyne-detection-with-silicon-field (visited on 06/24/2024).
8. A. Lisauskas, S. Boppel, M. Mundt, V. Krozer, and H. G. Roskos. "Subharmonic Mixing With Field-Effect Transistors: Theory and Experiment at 639 GHz High Above f_T". In: *IEEE Sensors Journal* 13.1 (Jan. 2013), pp. 124–132. ISSN: 1530-437X, 1558-1748. https://doi.org/10.1109/jsen.2012.2223668. URL: http://ieeexplore.ieee.org/document/6327585/ (visited on 07/15/2025).
9. F. Ludwig, J. Holstein, A. Krysl, A. Lisauskas, and H. G. Roskos. "Modeling of Antenna-Coupled Si MOSFETs in the Terahertz Frequency Range". In: *IEEE Transactions on Terahertz Science and Technology* 14.3 (May 2024), pp. 414–423. ISSN: 2156-342X, 2156-3446. https://doi.org/10.1109/TTHZ.2024.3388254. URL: https://ieeexplore.ieee.org/document/10497872/ (visited on 05/03/2024).
10. F. Ludwig, A. Generalov, J. Holstein, A. Murros, K. Viisanen, M. Prunnila, and H. G. Roskos. "Terahertz Detection with Graphene FETs: Photothermoelectric and Resistive Self-Mixing Contributions to the Detector Response". en. In: *ACS Applied Electronic Materials* (Mar. 2024), acsaelm.3c01511. ISSN: 2637-6113, 2637-6113. https://doi.org/10.1021/acsaelm.3c01511. URL: https://pubs.acs.org/doi/10.1021/acsaelm.3c01511 (visited on 03/28/2024).
11. S. Boppel, A. Lisauskas, M. Mundt, D. Seliuta, L. Minkevicius, I. Kasalynas, G. Valusis, M. Mittendor , S. Winnerl, V. Krozer, and H. G. Roskos. "CMOS Integrated Antenna-Coupled Field-Effect Transistors for the Detection of Radiation From 0.2 to 4.3 THz". en. In: *IEEE Transactions on Microwave Theory and Techniques* 60.12 (Dec. 2012), pp. 3834–3843. ISSN: 0018-9480, 1557-9670. https://doi.org/10.1109/TMTT.2012.2221732. URL: http://ieeexplore.ieee.org/document/6353608/ (visited on 06/15/2022).
12. A. Lisauskas, U. Pfeiffer, E. Öjefors, P. H. Bolìvar, D. Glaab, and H. G. Roskos. "Rational design of high-responsivity detectors of terahertz radiation based on distributed self-mixing in silicon field-effect transistors". en. In: *Journal of Applied Physics* 105.11 (June 2009), p. 114511. ISSN: 0021-8979, 1089-7550. https://doi.org/10.1063/1.3140611. URL: https://pubs.aip.org/jap/article/105/11/114511/147534/Rational-design-of-high-responsivity-detectors-of (visited on 05/16/2024).
13. E. Javadi, A. Lisauskas, M. Shahabadi, N. Masoumi, J. Zhang, J. Matukas, and H. G. Roskos. "Terahertz Detection With a Low-Cost Packaged GaAs High-Electron-Mobility Transistor". In: *IEEE Transactions on Terahertz Science and Technology* 9.1 (Jan. 2019), pp. 27–37. ISSN: 2156-342X, 2156-3446. https://doi.org/10.1109/TTHZ.2018.2877908. URL: https://ieeexplore.ieee.org/document/8506393/ (visited on 05/25/2023).
14. S. Regensburger, S. Preu, A. K. Mukherjee, S. Schonhuber, M. A. Kainz, S. Winnerl, J. M. Klopf, H. Lu, A. C. Gossard, and K. Unterrainer. " Broadband Terahertz Detection With Zero-Bias Field-Effect Transistors Between 100 GHz and 11.8 THz With a Noise Equivalent Power of 250 pW/sqrt(Hz) at 0.6 THz". In: *IEEE Transactions on Terahertz Science and Technology* 8.4 (July 2018), pp. 465–471. ISSN: 2156-342X, 2156-3446. https://doi.org/10.1109/TTHZ.2018.2843535. URL: https://ieeexplore.ieee.org/document/8371294/ (visited on 01/24/2024).
15. M. Bauer, A. Ramer, S. A. Chevtchenko, K. Y. Osipov, D. Cibiraite, S. Pralgauskaite, K. Ikamas, A. Lisauskas, W. Heinrich, V. Krozer, and H. G. Roskos. " A High-Sensitivity AlGaN/GaN HEMT Terahertz Detector With Integrated Broadband Bow-Tie Antenna". en. In: *IEEE Transactions on Terahertz Science and Technology* 9.4 (July 2019), pp. 430–444. ISSN: 2156-342X, 2156-3446. https://doi.org/10.1109/TTHZ.2019.2917782. URL: https://ieeexplore.ieee.org/document/8734725/ (visited on 06/15/2022).
16. Y. Sun, J. Sun, Y. Zhou, R. Tan, C. Zeng, W. Xue, H. Qin, B. Zhang, and D. Wu. " Room temperature GaN/AlGaN self-mixing terahertz detector enhanced by resonant antennas". In: *Applied Physics Letters* 98.15 (June 2013), p. 252103. https://doi.org/10.1063/1.3601489.
17. A. Zak, M. A. Andersson, M. Bauer, J. Matukas, A. Lisauskas, H. G. Roskos, and J. Stake. " Antenna-Integrated 0.6 THz FET Direct Detectors Based on CVD Graphene". en. In: *Nano Letters* 14.10 (Oct. 2014), pp. 5834–5838. ISSN: 1530-6984, 1530-6992. https://doi.org/10.1021/nl5027309. URL: https://pubs.acs.org/doi/10.1021/nl5027309 (visited on 06/15/2022).

18. A. A. Generalov, M. A. Andersson, X. Yang, A. Vorobiev, and J. Stake. "A 400-GHz Graphene FET Detector". en. In: *IEEE Transactions on Terahertz Science and Technology* 7.5 (Sept. 2017), pp. 614–616. ISSN: 2156-342X, 2156-3446. https://doi.org/10.1109/TTHZ.2017.2722360. URL: http://ieeexplore.ieee.org/document/7981343/ (visited on 06/15/2022).
19. M. Bauer, A. Lisauskas, P. Sakalas, M. Schröter, and H. Roskos. "Terahertz detection at 240 GHz with a semiconducting carbon-nanotube field-effect transistor". In: *39th Internat. Conf. on Infrared, Millimeter, and Terahertz Waves, Tuczon, AZ*. 2014. https://doi.org/10.1109/IRMMW-THz.2014.6956247.
20. K. Ikamas, D. Cibiraite, A. Lisauskas, M. Bauer, V. Krozer, and H. G. Roskos. "Broadband Terahertz Power Detectors Based on 90-nm Silicon CMOS Transistors With Flat Responsivity Up to 2.2 THz". In: *IEEE Electron Device Letters* 39.9 (Sept. 2018), pp. 1413–1416. ISSN: 0741-3106, 1558-0563. https://doi.org/10.1109/LED.2018.2859300. URL: https://ieeexplore.ieee.org/document/8418740/ (visited on 01/16/2023).
21. M. Ferreras, D. Cibiraite-Lukenskiene, A. Lisauskas, J. Grajal, and V. Krozer. " Broadband Sensing Around 1 THz Via a Novel Biquad-Antenna-Coupled Low-NEP Detector in CMOS". In: *IEEE Transactions on Terahertz Science and Technology* 11.1 (Jan. 2021), pp. 16–27. ISSN: 2156-342X, 2156-3446. https://doi.org/10.1109/TTHZ.2020.3031483. URL: https://ieeexplore.ieee.org/document/9226130/ (visited on 07/19/2022).
22. E. Ojefors, U. R. Pfeiffer, A. Lisauskas, and H. G. Roskos. " A 0.65 THz Focal-Plane Array in a Quarter-Micron CMOS Process Technology". In: *IEEE Journal of Solid-State Circuits* 44.7 (July 2009), pp. 1968–1976. ISSN: 0018-9200. https://doi.org/10.1109/JSSC.2009.2021911. URL: http://ieeexplore.ieee.org/document/5109781/ (visited on 01/13/2023).
23. F. F. Sizov, V. P. Reva, A. G. Golenkov, and V. V. Zabudsky. " Uncooled Detectors Challenges for THz/sub-THz Arrays Imaging". en. In: *Journal of Infrared, Millimeter, and Terahertz Waves* 32.10 (Oct. 2011), pp. 1192–1206. ISSN: 1866-6892, 1866-6906. https://doi.org/10.1007/s10762-011-9789-2. URL: http://link.springer.com/10.1007/s10762-011-9789-2 (visited on 07/09/2025).
24. R. Al Hadi, H. Sherry, J. Grzyb, Y. Zhao, W. Forster, H. M. Keller, A. Cathelin, A. Kaiser, and U. R. Pfeiffer. " A 1 k-Pixel Video Camera for 0.7–1.1 Terahertz Imaging Applications in 65-nm CMOS". In: *IEEE Journal of Solid-State Circuits* 47.12 (Dec. 2012), pp. 2999–3012. ISSN: 0018-9200, 1558-173X. https://doi.org/10.1109/JSSC.2012.2217851. URL: http://ieeexplore.ieee.org/document/6363486/ (visited on 03/21/2023).
25. J. Grzyb and U. Pfeiffer. " THz Direct Detector and Heterodyne Receiver Arrays in Silicon Nanoscale Technologies". en. In: *Journal of Infrared, Millimeter, and Terahertz Waves* 36.10 (Oct. 2015), pp. 998–1032. ISSN: 1866-6892, 1866-6906. https://doi.org/10.1007/s10762-015-0172-6. URL: http://link.springer.com/10.1007/s10762-015-0172-6 (visited on 03/21/2024).
26. J. Holstein, N. K. North, M. D. Horbury, S. Kondawar, I. Kundu, M. Salih, A. Krysl, L. Li, E. H. Linfield, J. R. Freeman, A. Valavanis, A. Lisauskas, and H. G. Roskos. " 8×8 Patch-Antenna-Coupled Tera-FET Detector Array for Terahertz Quantum-Cascade-Laser Applications". In: *IEEE Transactions on Terahertz Science and Technology* 14.6 (Nov. 2024), pp. 799–807. ISSN: 2156-342X, 2156-3446. https://doi.org/10.1109/TTHZ.2024.3438429. URL: https://ieeexplore.ieee.org/document/10623338/ (visited on 12/08/2024).
27. S. Boppel, A. Lisauskas, A. Max, V. Krozer, and H. G. Roskos. " CMOS detector arrays in a virtual 10-kilopixel camera for coherent terahertz real-time imaging". en. In: *Optics Letters* 37.4 (Feb. 2012), p. 536. ISSN: 0146-9592, 1539-4794. https://doi.org/10.1364/OL.37.000536. URL: https://opg.optica.org/abstract.cfm?URI=ol-37-4-536 (visited on 07/09/2024).
28. J. Zdanevicius, D. Cibiraite, K. Ikamas, M. Bauer, J. Matukas, A. Lisauskas, H. Richter, T. Hagelschuer, V. Krozer, H.-W. Hubers, and H. G. Roskos. " Field-Effect Transistor Based Detectors for Power Monitoring of THz Quantum Cascade Lasers". In: *IEEE Transactions on Terahertz Science and Technology* 8.6 (Nov. 2018), pp. 613–621. ISSN: 2156-342X, 2156-3446. https://doi.org/10.1109/TTHZ.2018.2871360. URL: https://ieeexplore.ieee.org/document/8536434/ (visited on 01/17/2023).
29. M. M. Wiecha, R. Kapoor, and H. G. Roskos. " Terahertz scattering-type near-field microscopy quantitatively determines the conductivity and charge carrier density of optically doped and impurity-doped silicon". In: *APL Photonics* 6.12 (Dec. 2021), p. 126108. https://doi.org/10.1063/5.0070608.
30. K. Ikamas, D. B. But, A. Cesiul, C. Kołaciński, T. Lisauskas, W. Knap, and A. Lisauskas. " All-Electronic Emitter-Detector Pairs for 250 GHz in Silicon". en. In: *Sensors* 21.17 (Aug. 2021), p. 5795. ISSN: 1424-8220. https://doi.org/10.3390/s21175795. URL: https://www.mdpi.com/1424-8220/21/17/5795 (visited on 12/04/2023).

31. A. Lisauskas, M. Bauer, S. Boppel, M. Mundt, B. Khamaisi, E. Socher, R. Venckevičius, L. Minkevičius, I. Kašalynas, D. Seliuta, G. Valušis, V. Krozer, and H. G. Roskos. “ Exploration of Terahertz Imaging with Silicon MOSFETs”. en. In: *Journal of Infrared, Millimeter, and Terahertz Waves* 35.1 (Jan. 2014), pp. 63–80. ISSN: 1866-6892, 1866-6906. https://doi.org/10.1007/s10762-013-0047-7. URL: http://link.springer.com/10.1007/s10762-013-0047-7 (visited on 01/16/2023).
32. M. Bauer, R. Venckevičius, I. Kašalynas, S. Boppel, M. Mundt, L. Minkevičius, A. Lisauskas, G. Valušis, V. Krozer, and H. G. Roskos. “ Antenna-coupled field-effect transistors for multi-spectral terahertz imaging up to 425 THz”. en. In: *Optics Express* 22.16 (Aug. 2014), p. 19235. ISSN: 1094-4087. https://doi.org/10.1364/OE.22.019235. URL: https://opg.optica.org/oe/abstract.cfm?uri=oe-22-16-19235 (visited on 05/19/2023).
33. N. K. North. “ High-Resolution Terahertz Gas Spectroscopy”. PhD thesis. Leeds, UK: University of Leeds, 2024. URL: https://etheses.whiterose.ac.uk/id/eprint/35969/ (visited on 02/19/2025).
34. M. D. Horbury, N. K. North, J. Holstein, H. Godden, L. H. Li, J. R. Freeman, E. H. Linfield, H. Roskos, A. Lisauskas, and A. Valavanis. “ Real-Time Terahertz Absorption Spectroscopy of Methanol and Deuterated-Methanol Vapour, using a TeraFET Detector Array”. In: *2023 48th Int. Conf. on Infrared, Millimeter, and Terahertz Waves (IRMMW-THz)*. Montreal, QC, Canada: IEEE, Sept. 2023, pp. 1–2. ISBN: 979-8-3503-3660-3. https://doi.org/10.1109/IRMMW-THz57677.2023.10298916. URL: https://ieeexplore.ieee.org/document/10298916/ (visited on 11/01/2023).
35. D. Čibiraitė-Lukenskienė, K. Ikamas, T. Lisauskas, V. Krozer, H. G. Roskos, and A. Lisauskas. “ Passive Detection and Imaging of Human Body Radiation Using an Uncooled Field-Effect Transistor-Based THz Detector”. en. In: *Sensors* 20.15 (July 2020), p. 4087. ISSN: 1424-8220. https://doi.org/10.3390/s20154087. URL: https://www.mdpi.com/1424-8220/20/15/4087 (visited on 10/24/2022).
36. A. Lisauskas, K. Ikamas, S. Massabeau, M. Bauer, D. Čibiraitė, J. Matukas, J. Mangeney, M. Mittendor, S. Winnerl, V. Krozer, and H. G. Roskos. “Field-effect transistors as electrically controllable nonlinear rectifiers for the characterization of terahertz pulses”. en. In: *APL Photonics* 3.5 (May 2018), p. 051705. ISSN: 2378-0967. https://doi.org/10.1063/1.5011392. URL: https://pubs.aip.org/app/article/3/5/051705/1024619/Field-effect-transistors-as-electrically (visited on 08/07/2024).
37. K. Ikamas, A. Lisauskas, S. Massabeau, M. Bauer, M. Burakevič, J. Vyšniauskas, D. Čibiraitė, V. Krozer, A. Rämer, S. Shevchenko, W. Heinrich, J. Tignon, S. Dhillon, J. Mangeney, and H. G. Roskos. “Sub-picosecond pulsed THz FET detector characterization in plasmonic detection regime based on autocorrelation technique”. In: *Semiconductor Science and Technology* 33.12 (Dec. 2018), p. 124013. ISSN: 0268-1242, 1361-6641. https://doi.org/10.1088/1361-6641/aae905. URL: https://iopscience.iop.org/article/10.1088/1361-6641/aae905 (visited on 11/13/2021).
38. D. Voss, W. Zouaghi, M. Jamshidifar, S. Boppel, C. McDonnell, J. R. P. Bain, N. Hempler, G. P. A. Malcolm, G. T. Maker, M. Bauer, A. Lisauskas, A. Rämer, S. A. Shevchenko, W. Heinrich, V. Krozer, and H. G. Roskos. “ Imaging and spectroscopic sensing with low-repetition-rate terahertz pulses and GaN TeraFET detectors”. In: *Journal of Infrared Millimeter and Terahertz Waves* 39.3 (Mar. 2018), pp. 262–272. https://doi.org/10.1007/s10762-017-0447-1.
39. N. K. North, M. D. Horbury, H. Godden, J. Holstein, I. Kundu, L. H. Li, S. Kondawar, E. H. Linfield, A. Valavanis, A. Lisauskas, and H. Roskos. “ Real-Time Terahertz Transmission Spectroscopy of Deuterium Exchange between Methanol and Deuterated Water in the Gas-Phase”. to be submitted. 2025.
40. M. Andree, J. Grzyb, H. Rücker, and U. R. Pfeifier. “Towards Passive Imaging With Uncooled, Low-NEP SiGe HBT Terahertz Direct Detectors”. In: *IEEE Transactions on Terahertz Science and Technology* 14.5 (Sept. 2024), pp. 632–651. ISSN: 2156-342X, 2156-3446. https://doi.org/10.1109/TTHZ.2024.3432619. URL: https://ieeexplore.ieee.org/document/10607950/ (visited on 10/14/2024).
41. H. Yuan, Q. Ul-Islam, and H. G. Roskos. “ Superstrate-lens integration using paraffin wax on top of semiconductor-based THz detector chips”. In: *Lithuanian Journal of Physics* 63.4 (Dec. 2023). ISSN: 2424-3647, 1648-8504. https://doi.org/10.3952/physics.2023.63.4.6. URL: https://lmaleidykla.lt/ojs/index.php/physics/article/view/5198 (visited on 10/25/2024).
42. J. Van Rudd and D. M. Mittleman. “ Influence of substratelens design in terahertz time-domain spectroscopy”. en. In: *Journal of the Optical Society of America* B 19.2 (Feb. 2002), p. 319. ISSN: 0740-3224, 1520-8540. https://doi.org/10.1364/JOSAB.19.000319. URL: https://opg.optica.org/abstract.cfm?URI=josab-19-2-319 (visited on 12/08/2023).
43. A. Lisauskas, S. Boppel, J. Matukas, V. Palenskis, L. Minkevičius, G. Valušis, P. Haring-Bolíar, and H. G. Roskos. “ Terahertz responsivity and low-frequency noise in biased silicon field-effect transistors”.

en. In: *Applied Physics Letters* 102.15 (Apr. 2013), p. 153505. ISSN: 0003-6951, 1077-3118. https://doi.org/10.1063/1.4802208. URL: https://pubs.aip.org/aip/apl/article/125983 (visited on 10/16/2024).
44. A. J. Deninger, A. Roggenbuck, S. Schindler, and S. Preu. " 2.75 THz tuning with a triple-DFB laser system at 1550 nm and InGaAs photomixers". en. In: *Journal of Infrared, Millimeter, and Terahertz Waves* 36.3 (Mar. 2015), pp. 269–277. ISSN: 1866-6892, 1866-6906. https://doi.org/10.1007/s10762-014-0125-5. URL: http://link.springer.com/10.1007/s10762-014-0125-5 (visited on 04/21/2022).
45. About Lock-In Amplifiers. Tech. rep. Stanford Research Systems (SRS), 2022.
46. M. Ferreras Mayo. " Design and experimental validation of antenna-coupled devices for terahertz applications". PhD Thesis. Universidad Politécnica de Madrid, Feb. 2023. https://doi.org/10.20868/UPM.thesis.72960. URL: http://oa.upm.es/72960/ (visited on 10/04/2023).
47. J. Holstein, A. Krysl, D. B. But, K. Ikamas, A. Lisauskas, and H. G. Roskos. " Patch-antenna-coupled TeraFET detector State-of-the-art sensitivity by effective radiation focusing with a low-loss superstrate lens". In: *2024 49th IRMMW-THz*. Perth, Australia: IEEE, Sept. 2024, pp. 1–2. ISBN: 979-8-3503-7032-4. https://doi.org/10.1109/IRMMW-THz60956.2024.10697756. URL: https://ieeexplore.ieee.org/document/10697756/ (visited on 11/03/2024).
48. M. Kocybik, M. Bauer, and F. Friederich. " Parasitic mixing in photomixers as continuous wave terahertz sources". en. In: *Scientific Reports* 14.1 (Mar. 2024), p. 5534. ISSN: 2045-2322. https://doi.org/10.1038/s41598-024-55661-x. URL: https://www.nature.com/articles/s41598-024-55661-x (visited on 04/22/2024).
49. P. Ourednik, D. Theiner, G. Picco, K. Unterrainer, and M. Feiginov. " Dynamic range limitations of non-coherent continous-wave THz photomixing systems with broadband detectors". en. In: *Optics Express* 32.22 (Oct. 2024), p. 38344. ISSN: 1094-4087. https://doi.org/10.1364/oe.537340. URL: https://opg.optica.org/abstract.cfm?URI=oe-32-22-38344 (visited on 07/08/2025).
50. *Silicon MEMS Optical Technology Infrared Emitters*. Tech. rep. Electro Optical Components, Inc., Dec. 2025. URL: https://eoc-inc.com/wp-content/uploads/2018/11/INTEX-Brochure-0511.pdf (visited on 12/25/2025).
51. AMETEK ADVANCED MEASUREMENT TECHNOLOGY, INC. *Model 7265 DSP Lock-in Amplifier - Instruction Manual*. 2002.
52. D. J. Schroeder. *Astronomical optics*. 2nd ed. San Diego: Academic Press, 2000. ISBN: 978-0-12-629810-9.
53. M. Ali, M. Perenzoni, and D. Stoppa. " A Methodology to Measure Input Power and Effective Area for Characterization of Direct THz Detectors". In: *IEEE Transactions on Instrumentation and Measurement* 65.5 (May 2016), pp. 1225–1231. ISSN: 0018-9456, 1557-9662. https://doi.org/10.1109/TIM.2016.2534199. URL: http://ieeexplore.ieee.org/document/7434606/ (visited on 05/25/2023).
54. F. Ludwig. " Terahertz detection with field-effect transistors: experimental characterization and hydrodynamic modeling". PhD thesis. Frankfurt am Main: Johann Wolfgang Goethe-Universität, 2024. URL: https://publikationen.ub.unifrankfurt.de/frontdoor/index/index/docId/93123 (visited on 10/17/2025).
55. R. U. Titz, H. P. Röser, G. W. Schwaab, H. J. Neilson, P. A. Wood, T. W. Crowe, W. C. B. Peatman, J. Prince, B. S. Deaver, H. Alius, and G. Dodel. " Investigation of GaAs Schottky barrier diodes in the THz range". en. In: *International Journal of Infrared and Millimeter Waves* 11.7 (July 1990), pp. 809–820. ISSN: 0195-9271, 1572-9559. https://doi.org/10.1007/BF01010134. URL: http://link.springer.com/10.1007/BF01010134 (visited on 04/11/2025)
56. W. C. B. Peatman, P. A. D.Wood, D. Porterfield, T. W. Crowe, and M. J. Rooks. "Quarter-micrometer GaAs Schottky barrier diode with high video responsivity at 118 um". en. In: *Applied Physics Letters* 61.3 (July 1992), pp. 294–296. ISSN: 0003-6951, 1077-3118. https://doi.org/10.1063/1.107944. URL: https://pubs.aip.org/apl/article/61/3/294/61273/Quarter-micrometer-GaAs-Schottky-barrier-diode (visited on 04/11/2025).
57. H.-W. Hübers, G. W. Schwaab, and H. P. Röser. "Video detection and mixing performance of GaAs Schottky-barrier diodes at 30 THz and comparison with metal-insulator-metal diodes". en. In: *Journal of Applied Physics* 75.8 (Apr. 1994), pp. 4243–4248. ISSN: 0021-8979, 1089-7550. https://doi.org/10.1063/1.355980. URL: https://pubs.aip.org/jap/article/75/8/4243/951/Video-detection-and-mixingperformance-of-GaAs (visited on 04/10/2025).
58. R. Jain, R. Zatta, J. Grzyb, D. Harame, and U. Pfeiffer. " A Terahertz Direct Detector in 22nm FD-SOI CMOS". en. In: *2018 13th European Microwave Integrated Circuits Conference (EuMIC)* (2018), pp. 25–28. https://doi.org/10.23919/EuMIC.2018.8539908. URL: https://elpub.bib.uni-wuppertal.de/receive/duepublico_mods_00000754 (visited on 08/31/2024).

59. C. Elmaleh, F. Simon, J. Decker, J. Dumont, F. Cazier, M. Fourmentin, R. Bocquet, A. Cuisset, G. Mouret, and F. Hindle. " THz cavity ring-down quantitative gas phase spectroscopy". en. In: *Talanta* 253 (Feb. 2023), p. 124097. ISSN: 00399140. https://doi.org/10.1016/j.talanta.2022.124097. URL: https://linkinghub.elsevier.com/retrieve/pii/S0039914022008931 (visited on 11/20/2025).
60. Virginia Diodes, Inc.. *Zero Bias Detector (ZBD/ZBD-F)*. Oct. 2025. URL: https://www.vadiodes.com/en/products/detectors (visited on 07/15/2025).
61. B. T. Bulcha, J. L. Hesler, V. Drakinskiy, J. Stake, A. Valavanis, P. Dean, L. H. Li, and N. S. Barker. " Design and Characterization of 1.8–3.2 THz Schottky-Based Harmonic Mixers". In: *IEEE Transactions on Terahertz Science and Technology* 6.5 (Sept. 2016), pp. 737–746. ISSN: 2156-342X, 2156-3446. https://doi.org/10.1109/TTHZ.2016.2576686. URL: https://ieeexplore.ieee.org/document/7533505/ (visited on 04/17/2025).
62. R. Yadav, F. Ludwig, F. R. Faridi, J. M. Klopf, H. G. Roskos, S. Preu, and A. Penirschke. " State-of-the-Art Room Temperature Operable Zero-Bias Schottky Diode-Based Terahertz Detector Up to 5.56 THz". en. In: *Sensors* 23.7 (Mar. 2023), p. 3469. ISSN: 1424-8220. https://doi.org/10.3390/s23073469. URL: https://www.mdpi.com/1424-8220/23/7/3469 (visited on 04/08/2024).
63. Z. Ahmad, A. Lisauskas, H. G. Roskos, and K. O. "Design and demonstration of antenna-coupled Schottky diodes in a foundry complementary metal-oxide semiconductor technology for electronic detection of far-infrared radiation". In: *Journal of Applied Physics* 125.19 (May 2019), p. 194501. https://doi.org/10.1063/1.5083689.
64. B. Drouin, D. Nemchick, and A. Maestrini. " High precision measurement of the 3P0 - 3P1 atomic oxygen fine structure splitting at 2.06 THz". en. In: *Journal of Quantitative Spectroscopy and Radiative Transfer* 342 (Sept. 2025), p. 109471. ISSN: 00224073. https://doi.org/10.1016/j.jqsrt.2025.109471. URL: https://linkinghub.elsevier.com/retrieve/pii/S0022407325001335 (visited on 09/23/2025).
65. J. Elumalai, M. Salih, M. Fice, A. Brown, L. Li, E. H. Linfield, A. Valavanis, A. J. Seeds, A. G. Davies, and J. R. Freeman. " Free-space optical communications at 4 Gbit/s data rate with a terahertz laser". en. In: *Communications Physics* 9.1 (Feb. 2026), p. 33. ISSN: 2399-3650. https://doi.org/10.1038/s42005-025-02471-w. URL: https://www.nature.com/articles/s42005-025-02471-w (visited on 02/13/2026).

Authors and Affiliations

Jakob Holstein[1] · **Dmytro B. But**[2,3] · **Anastasiya Krysl**[1] · **Alvydas Lisauskas**[1,4,5] · **Hartmut G. Roskos**[1]

✉ Jakob Holstein
holstein@physik.uni-frankfurt.de

Hartmut G. Roskos
roskos@physik.uni-frankfurt.de

1 Physikalisches Institut, Johann Wolfgang Goethe-Universität, Frankfurt am Main 60438, Germany

2 CENTERA Laboratories, Institute of High-Pressure Physics PAS, Warsaw 01-142, Poland

3 IB1, National Centre for Nuclear Research Świerk, Otwock 05-400, Poland

4 Institute of Applied Electrodynamics and Telecommunications, Vilnius University, Vilnius 10257, Lithuania

5 Center for Physical Sciences and Technology, Vilnius 10257, Lithuania